ADVANCING EARTH AND SPACE SCIENCES

JGR Atmospheres

RESEARCH ARTICLE
10.1029/2024JD041899

Special Collection:
Land-atmosphere coupling: measurement, modelling and analysis

Spatial Variability of the Response of Land-Atmosphere Coupling to Climate Warming in Northern China

Q. Zhang[1,2], L. Zhang[1], J. Zeng[3], Z. Yang[3], J. Zhao[1], F. Zhao[1], S. Wang[1], S. Sha[1], and J. Wang[1]

[1]Key Laboratory of Arid Climatic Change and Reducing Disaster of Gansu Province, Key Open Laboratory of Arid Climatic Change and Disaster Reduction of CMA, Institute of Arid Meteorology, CMA, Lanzhou, China, [2]Gansu Meteorological Bureau, Lanzhou, China, [3]School of Atmospheric Sciences, Chengdu University of Information Technology, Chengdu, China

Key Points:

- Northern China exhibits intense land-atmosphere coupling due to varied features, resulting in noticeable feedbacks
- The research examined how land-atmosphere coupling processes react to climate warming and spatial changes in northern China
- The study uncovered coupling responses affected by energy and moisture, with the SMTR exhibiting mixed feedbacks to climate warming

Correspondence to:

L. Zhang,
lzhangmet@163.com

Citation:

Zhang, Q., Zhang, L., Zeng, J., Yang, Z., Zhao, J., Zhao, F., et al. (2025). Spatial variability of the response of land-atmosphere coupling to climate warming in northern China. *Journal of Geophysical Research: Atmospheres*, *130*, e2024JD041899. https://doi.org/10.1029/2024JD041899

Received 30 JUN 2024
Accepted 5 MAY 2025

Author Contributions:

Conceptualization: Q. Zhang
Data curation: L. Zhang, S. Wang, S. Sha, J. Wang
Investigation: L. Zhang, J. Zhao
Methodology: Q. Zhang, L. Zhang
Project administration: Q. Zhang, L. Zhang, S. Wang
Resources: F. Zhao, J. Wang
Software: S. Sha
Supervision: J. Zeng, J. Zhao, F. Zhao
Validation: L. Zhang
Visualization: Z. Yang
Writing – original draft: Q. Zhang

Abstract Northern China is a global hotspot for intense land-atmosphere coupling because its atmospheric and land-surface features vary substantially, making the mutual feedbacks and linked responses between coupling variables more prominent. Based on Global Land Data Assimilation System (GLDAS) data, land grid data from ECMWF Re-Analysis project data-Interim (ERA-Interim), ECMWF Scheme for Surface Exchanges over Land incorporating land surface hydrology (ERA5-land) and Global Land Evaporation Amsterdam Model 4 (GLEAM4) global land flux network (FLUXNET) data and weather observation data, the variability of the response of land-atmosphere coupling processes to climate warming with the spatial change of the climate background in northern China was analyzed. The response mechanisms of the coupling processes between land evapotranspiration and soil moisture, and between surface net radiation and soil moisture to the spatial change of precipitation climate space (defined by the annual mean value of a given physical quantity) were investigated. Additionally, the effect of climate space on land-atmosphere coupling characteristics was investigated. Results indicate that there were significant spatial differences in the trends of temperature and precipitation variation in northern China, and the characteristics of land-atmosphere coupling in response to climate change were strongly reliant on the energy and moisture constraints in climate space. The summer monsoon transitional region (SMTR) was found to be a climate-sensitive zone with competition between moisture and energy, where the response of land-surface physical quantities to climate change underwent a radical transformation, and land-atmosphere coupling processes displayed both positive feedback (temperature increasing→soil moisture decreasing→net radiation decreasing→temperature increasing) and negative feedback (temperature increasing→soil moisture decreasing→net radiation increasing→temperature decreasing) to climate warming. These findings would improve the scientific understanding of the characteristics and mechanisms of land-atmosphere coupling processes for a heterogeneous underlying surface, and may provide an important theoretical basis for climate prediction in northern China.

Plain Language Summary Northern China has intense interactions between the land and atmosphere due to its varying climate and land features. This study analyzed how these interactions respond to climate warming across different regions in northern China using multiple data sources. The study found that temperature and precipitation trends varied significantly across the region, and the response of land-atmosphere coupling to climate change depended on the energy and moisture constraints in the climate space. The summer monsoon transitional region was identified as a climate-sensitive zone where the response of land-surface physical quantities to climate change underwent significant changes, and land-atmosphere coupling processes displayed both positive and negative feedbacks to climate warming. The results of this study improves our understanding of the characteristics and mechanisms of land-atmosphere coupling processes in areas with varying climate and land features, and may provide a theoretical basis for climate prediction in northern China.

1. Introduction

Land-atmosphere coupling processes are very important for the exchange of energy, water, and momentum between the land surface and atmosphere, and play a significant role in atmospheric convection (Zheng et al., 2015), cloud physical processes (Min et al., 2022), and the formation of local circulation (Schumacher et al., 2019). The mutual feedback process between soil moisture and precipitation through land evapotranspiration is an important means of land-atmosphere coupling, and can significantly affect weather, climate, and climate change (Seneviratne et al., 2016). The mutual feedback process is also relatively poorly understood in

Writing – review & editing: L. Zhang, J. Zeng, Z. Yang, J. Zhao, S. Wang

terms of the formation and development mechanisms of extreme weather, climate events, and meteorological disasters (Taylor et al., 2011; Zhou et al., 2019). Thus, land-atmosphere coupling processes have become a hot research topic worldwide in recent years.

Land-atmosphere coupling processes mainly consist of the energy and hydrological cycles between the land surface and atmosphere as well as their correlations. The characteristics and action mechanisms of the coupling processes are not only affected by atmospheric background factors such as wind speed, precipitation, temperature, humidity, air pressure, and solar radiation, but are also associated with land-surface conditions, such as soil moisture, soil properties, and vegetation coverage (Seneviratne et al., 2006). Land-atmosphere coupling processes are therefore highly dependent on the spatial and temporal changes of climatic and environmental conditions (Wetzel et al., 1996). The spatial differences in climatic background and the geographical environment can often cause a distinct spatial variability in the characteristics of land-atmosphere coupling processes. Air temperature is the most active climate element, and therefore land-atmosphere coupling processes will respond significantly to temperature warming, which exhibits notable spatial variations (Wang & Zeng, 2015).

Previous studies showed that the response of regional land-atmosphere coupling to global warming differed substantially under the different climates, and different climatic zones even show the opposite response trends or mutual feedback relationships (Evans et al., 2011; Guo & Dirmeyer, 2013; Seneviratne et al., 2010). This not only indicates the complex relationship between land-atmosphere coupling processes and the weather and climate, but also emphasizes the difficulty in understanding the characteristics and action mechanisms of land-atmosphere coupling. In the humid summer monsoon region, heatwaves weather leads to soil moisture affecting net long-wave radiation and sensible heat flux at the surface, which in turn creates favorable land conditions for the persistence of heatwaves (Ni et al., 2024; Wang et al., 2024). In the northern arid region, strong surface sensible heat flux and the entrainment effect of residual layer energy result in a significantly higher convective boundary layer height compared to other climatic regions (Freire & Dias, 2013; B. Carreras et al., 2014), with a maximum value reaching 4,170 m (Zhang, Qiao, et al., 2019). In the summer monsoon transition region, the long-term accumulative effect of shallow soil moisture and boundary layer land-atmosphere dry thermal coupling contributes significantly to deep soil drought on a cross-seasonal scale. Clearly, the land-atmosphere coupling processes in northern China are complex and exhibit significant spatial climatic differences. Many scientific issues in this field remain unsolved, which has seriously limited the ability to understand the characteristics and mechanisms of land-atmosphere coupling. Some of the unanswered questions include: What are the land-atmosphere coupling characteristics with the spatial variation of climatic background? What factors influence the relationship between land-atmosphere coupling characteristics and the climatic background? Under what specific climate conditions will there be a positive or negative feedback between evapotranspiration and soil moisture content?

Northern China is characterized by the frequent convergence of the East Asian summer monsoon, the Northern Hemisphere westerly jet stream, and high-latitude cold air masses. This distinctive atmospheric circulation results in a region encompassing humid, semi-arid, and arid climates, with pronounced spatial transitions (Zhang et al., 2016). The unique spatial climate characteristics lead to a vegetation pattern that transitions from deciduous broadleaf forests in the southeast to desert grasslands in the northwest (Zhang, Qiao, et al., 2019). The region's sensitivity to precipitation variability contributes to the frequent occurrence of extreme weather events as the climate warms. With the East Asian summer monsoon and its special geographical environmental conditions, northern China is known to be a global center of land-atmosphere coupling (Koster et al., 2004), and is very sensitive to global warming. This is likely to be a major reason for the frequent occurrence of drought disasters and the worsening drought conditions in this region (Han et al., 2021). Based on the activities of the Asian summer monsoon, northern China can be divided into three typical climate zones, namely, a summer monsoon region (SMR), summer monsoon transitional region (SMTR), and non-summer monsoon region (NSMR) (Figure 1), where agricultural-pastoral ecotones, climatic transition zones, and other regions with very notable temporal and spatial changes in climatic background and geographical conditions are widely distributed (Zhang et al., 2014). Changes in the spatial gradient of the climate background, soil moisture conditions, and vegetation coverage in this region can lead to changes in land-surface energy and moisture exchange processes. In particular, land-surface evapotranspiration and net radiation have a very sensitive response to these kinds of spatial variations (Taylor et al., 2011), which will further aggravate the complexity of the spatial distribution of climate and soil conditions (Emori, 1998). Because northern China is sensitive to climate change, the mechanisms by which land-atmosphere coupling processes respond to climate warming are affected by the local climate space, and a

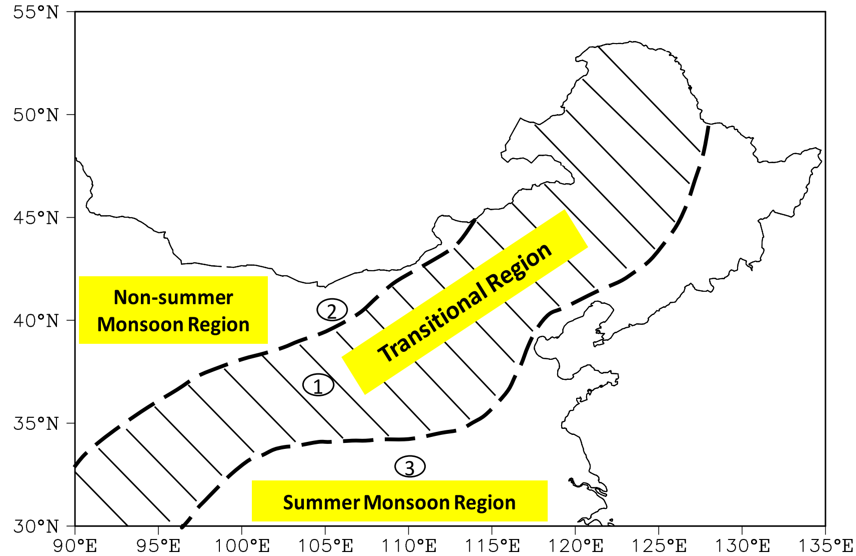

Figure 1. Schematic diagram of the study area (the numbers in circles represent the location of field observation stations: Yuzhong, Yan'an, Shangluo).

significant transformation of these mechanisms is possible (Zhang, Yang, et al., 2019). These phenomena make the problem of climatic spatial variability in land-atmosphere coupling processes over northern China more noticeable, resulting in more factors influencing weather forecasting and climate prediction in northern China (Findell & Eltahir, 2003a, 2003b; Rihani et al., 2015).

Some researchers have studied the response of land-atmosphere coupling processes to climate change in northern China (Li et al., 2021), and a certain scientific understanding of the mutual feedback processes between land evapotranspiration and air temperature has been achieved (Zhang, Yang, et al., 2019; L. Zhang et al., 2022, Q. Zhang et al., 2022). However, previous studies focused more on the multi-scale response of the physical quantities of land surface processes in northern China to the East Asian summer monsoon (Zhang et al., 2016, 2020, 2021). Less attention has been given to the unique land-atmosphere coupling characteristics in this region although a few studies have considered the complex mutual feedback processes between soil moisture and land evapotranspiration (Liu et al., 2014; Zuo & Zhang, 2016). Moreover, what are the characteristics of the key soil moisture-evapotranspiration processes in land-atmosphere coupling in northern China? How do the response characteristics of land-atmosphere coupling processes to climate warming change with spatial variations in climate? There has been no scientific recognition. This situation has restricted our understanding of the function of land-atmosphere coupling in the formation and development mechanisms of extreme weather and climate events in northern China, and also restricted the accuracy of forecasting convective precipitation in this region.

In recent years, the level of land-air interaction collaborative observations and the reliability of data for northern China have significantly improved (Huang et al., 2012; Liu et al., 2011). Additionally, the multi-model simulation level of the Global Land Data Assimilation System (GLDAS) and the land-surface data reanalysis technology have been continuously improved worldwide (Wei et al., 2015), providing sufficient data support for the study of the response variability of land-atmosphere coupling processes to climate warming in northern China under the context of varying climate space. To better understand the characteristics and mechanisms of land-atmosphere coupling in the climatic and ecological transition zones and provide the basic theoretical basis for improving the accuracy of weather forecasts and climate prediction in northern China, we are to analyze the trends of temperature and precipitation variation in northern China alongside the variation of climate space, and explore the response variability characteristics of land-atmosphere coupling processes to climate warming in an attempt to determine the factors regulating the response of the mutual feedback processes between land evapotranspiration and soil moisture and between surface net radiation and soil moisture to the changes in precipitation climate space. The characteristic features of the transformation of land-atmosphere coupling mechanisms with the variation of climate space will also be identified.

Table 1
Details of the Data Used in This Study

Data types	Spatial resolution (°)	Temporal resolution	Time scale (year)
FLUXNET-Evapotranspiration	1.0° × 1.0°	Month	1982–2014
CAMSMD-Observed Soil Moisture	Stations	Ten days	1981–2009
CRU-Precipitation, Tair	0.5° × 0.5°	Month	1901–2018
ERA-Interim Soil Moisture	0.5° × 0.5°	Month	1979–2018
GLDAS 1	1.0° × 1.0°	Month	1979–2019
ERA5-land	0.1° × 0.1°	Month	1950–5 days before the current day
GLEAM4	0.25° × 0.25°	Month	1980-present

2. Data and Methods

2.1. Study Area

The study area is the region north of the Yangtze River and west of Xinjiang in northern China, as shown in Figure 1. This region features the most prominent transition of the Asian summer monsoon, with extensive agricultural and pastoral ecotones and is located within a climatic transition zone. According to the extent of the influence of the summer monsoon, it can be divided into the three typical climate regions of SMR, SMTR, and NSMR, and its climate background and geographical environment conditions vary substantially in time and space (Zhang et al., 2014). This region, which is very sensitive to climate change, has strong incoming solar radiation, a large land evaporation potential, and a distinct spatio-temporal variation of precipitation as well as a fragile ecology. In this region, there are significant spatial differences in the soil moisture content and vegetation coverage, which change over a distinct annual-cycle with large interannual fluctuations.

2.2. Data

The study used climatic data such as temperature and precipitation, and land-surface process data including soil moisture, land evapotranspiration, and surface net radiation. These data selected from multi-source data sets available worldwide can meet the requirements of this study in terms of data accuracy, continuity, integrity, and reliability, as well as time series length (Table 1). The temperature and precipitation data were derived from the Climatic Research Unit (CRU) data set (Harris et al., 2014) and the data reliability has been confirmed. Characterized by long time series, good integrity, high reliability, and the quantitative description of the data for the climate state has been verified (Zhang et al., 2017), thus the data were widely used in climatological research (Sheffield et al., 2006; Zhang et al., 2011, 2017). The data used in this study were the TS v4 version recently released by CRU, covering the period of 1901–2018 (Harris et al., 2020). The observed soil moisture was derived from China Agricultural Meteorological Soil Moisture Data set (CAMSMD, Zhang et al., 2017).

The land evapotranspiration data were from the global FLUXNET grid data set, which were made by the German Max Planck Institute of Biogeochemistry based on global land surface flux observations through strict quality control testing, machine learning verification, and spatial up-scaling processing (Pastorello et al., 2021). Covering the period of 1982–2014, the data have the advantages of a long time series and good compatibility with global climate data, and are often used in studies of land-atmosphere interaction (Jung et al., 2009; Zeng & Zhang, 2012). Moreover, one study has demonstrated that this data can reflect the spatial characteristics of land-atmosphere interactions in northern China (Zhang, Yang, et al., 2019). The model-based evapotranspiration data were obtained from GLDAS, ERA-Interim, ERA5-Land, and GLEAM4. ERA5-Land has been produced by replaying the land component of the ECMWF ERA5 climate reanalysis, with its evapotranspiration data sourced from the Penman-Monteith equation (Hersbach et al., 2020). GLEAM4 is a hybrid evaporation model that harnesses the synergy between process-based modeling and machine learning. In GLEAM4, earlier empirical evaporative stress functions were replaced by deep neural networks trained on eddy-covariance and sapflow data to better represent the complex physiological response of vegetation to multiple environmental stressors (Martens et al., 2017; Miralles et al., 2011). Further information is shown in Table 1.

The land-surface soil moisture data were obtained from GLDAS (Rodell et al., 2004) ERA-Interim, ERA5-land, and GLEAM4 global reanalysis grid data. The GLDAS data has been publicly released in two versions: GLDAS 1

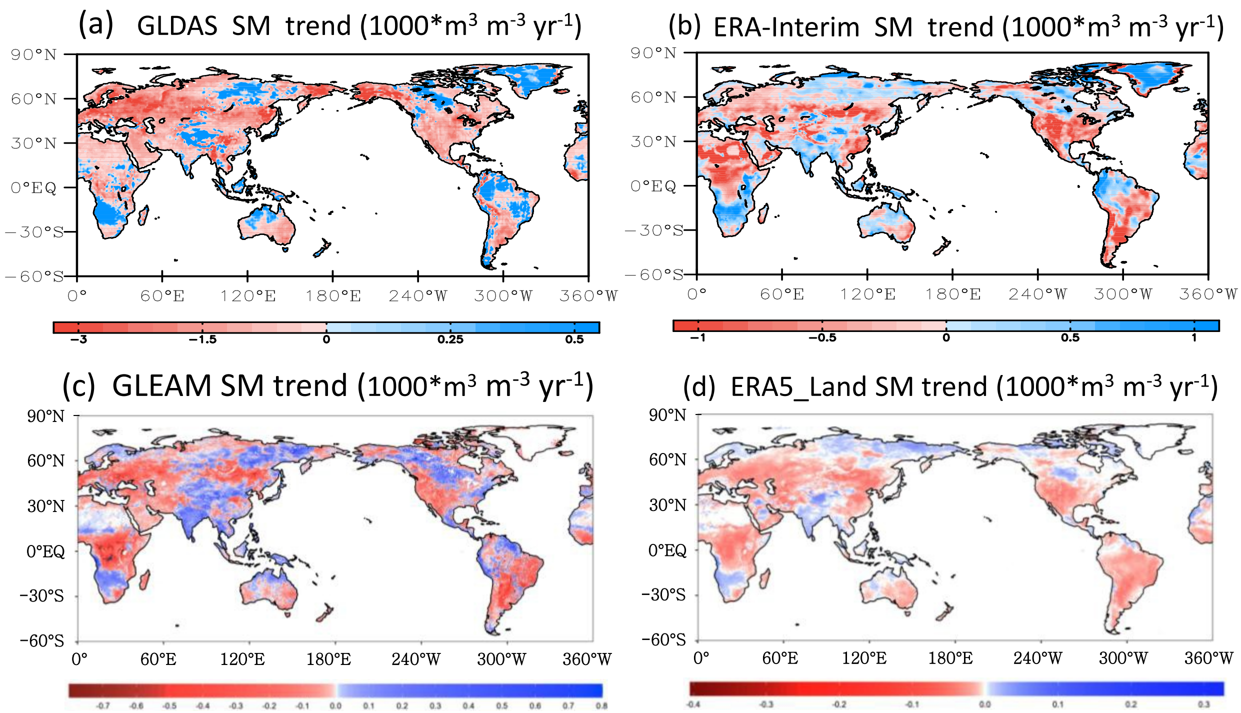

Figure 2. Global distribution of soil moisture inclination rates from (a) GLDAS, (b) EAR-Interim, (c) GLEAM4 and (d) ERA5-Land data. All inclination rates passed the significance test at the 95% confidence levels.

and GLDAS 2. The GLDAS 2 data are newer than the GLDAS 1 data, but its time series is short, only from the year 2000 to the present. In contrast, the GLDAS 1 data consist of more model simulation results with a longer time series (from January 1979 to April 2020), and can be better matched with climate data and land evapotranspiration data. Zhang et al. (2014) indicated that the land surface models that provides simulation results for GLDAS 1 data can perform well in simulating the spatial distribution patterns of the land surface fluxes in northern China. To further reduce the uncertainty caused by the different models, we used an ensemble mean of the four GLDAS 1 models in this research, which effectively reduces the systematic errors of the land-surface flux data. The ERA-Interim (ECMWF Re-Analysis project data-Interim) data are a set of high-resolution reanalysis data released by the European Center for Medium-range Weather Forecasting (ECMWF) (Berrisford et al., 2011). This is the land surface data obtained by improving the hydrological and energy cycle processes of land surface process models on the basis of an ECMWF Re-Analysis describing the state of the global atmosphere and land conditions for 45-year (ERA-40). The GLEAM soil moisture data are a set of algorithms dedicated to the estimation of root-zone soil moisture from satellite data (Martens et al., 2017). To mitigate the adverse effects of discrepancies in soil layers and thicknesses among GLDAS, ERA-Interim, and ERA5-Land, this study focuses on soil moisture data interpolated to a depth of 0–40 cm. Consequently, these data sets were employed to analyze the response and feedback mechanisms of soil moisture to climate warming.

2.3. Comparative Verification of Soil Moisture Data

The soil moisture and land evapotranspiration are the land surface elements that are more sensitive to climate change. The verified global FLUXNET data of land evapotranspiration in northern China are selected because it is more reliable than other similar data available internationally (Zhang, Yang, et al., 2019).

Figure 2 compares the trends of soil moisture variation from GLDAS ERA-Interim, GLEAM4 and ERA5-Land data. The changes in the soil moisture content in the GLDAS data show that the range of global drying was more extensive than that for global wetting (Figure 2a), and that the drying areas were mainly concentrated in the Northern Hemisphere. Among the high-latitude regions in the Northern Hemisphere, the Qinghai-Tibet Plateau in China, Greenland, and the Central and Western Siberian Plateau exhibit the most significant wetting trends (Feng & Fu, 2013). In contrast, the extent of land drying and wetting in the Southern Hemisphere is not as prominent as

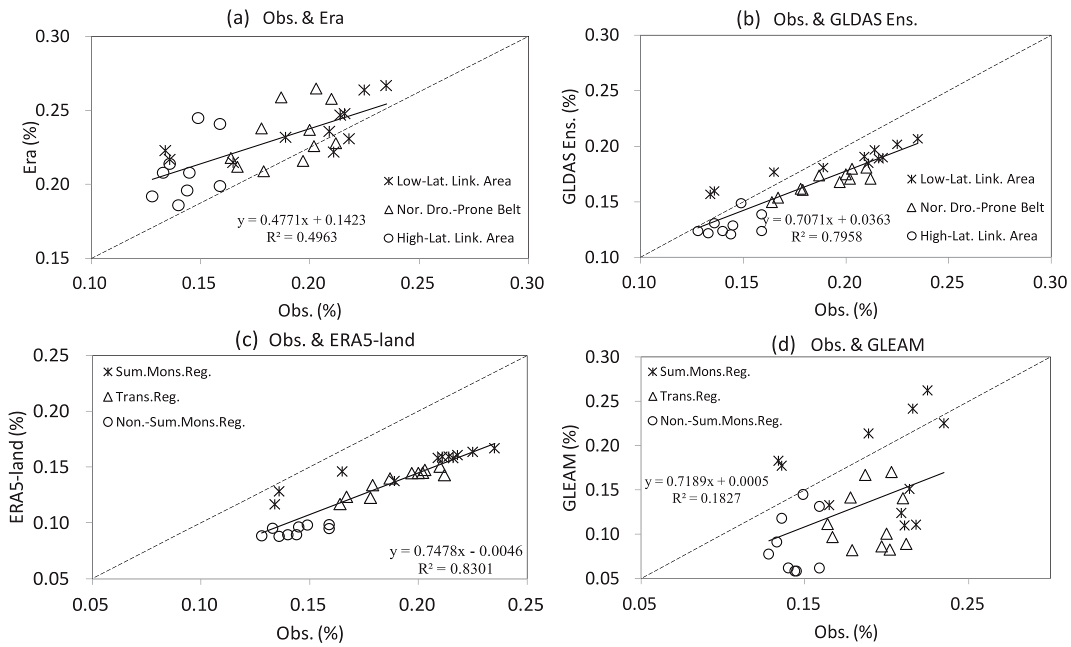

Figure 3. Correlation of (a) ERA-interim, (b) GLDAS, (c) ERA5-land and (d) GLEAM4 soil moisture data with the observed soil moisture derived from CAMSMD.

in the boreal hemisphere, and the spatial drying and wetting trends are also more uniform. These characteristics have been verified in previous studies (Deng et al., 2020).

Compared to the GLDAS soil moisture data, the ERA-Interim and ERA5-Land soil moisture data captured the characteristics of the major global surface drying areas better (Figures 2b and 2d), but the range of soil moisture values in the ERA-Interim and ERA5-Land data was too wide and the degree of soil wetting was too high (Cheng & Huang, 2016; Deng et al., 2020). In particular, for the change of soil moisture in the climate transitional zone, the ERA-Interim and ERA5-Land data were not dependable (Cheng & Huang, 2016), which resulted in errors in the ERA-Interim data for northern China. Moreover, the degree of soil wetting in the GLEAM4 data were higher than that in ERA-Interim and ERA5-Land in northern China (Figure 2c). Therefore, the GLDAS data could more objectively reflect the climate pattern of soil moisture in northern China and its response to climate warming.

To better understand the strengths and weaknesses of GLDAS, ERA-interim, ERA5-land and GLEAM4 soil moisture data, we compared them with the observed soil moisture data from the three observation stations in northern China in Figure 1, with the results shown in Figure 3. The GLDAS data, ERA-interim data, and ERA5-land data were well correlated with the observations, with determination coefficients (R^2) of 0.79, 0.49 and 0.83, respectively. In comparison, the GLDAS and ERA5-land soil moisture data were much closer to the observations and had stronger correlations. Table 2 lists the statistical parameters used to test and compare the three climate zones (SMR, SMTR, and NSMR), further illustrating that the correlation coefficient and root mean square error (RMSE) between GLDAS soil moisture data and the observations were significantly superior to those of the

Table 2
Statistical Parameters for the Testing and Comparison of GLDAS, ERA-Interim, ERA5-Land and GLEAM4 Soil Moisture Data With Observations in Different Climate Zones

	Temporal correlation				RMSE (%)			
	GLDAS	ERA-interim	ERA5-land	GLEAM4	GLDAS	ERA-interim	Era5-land	GLEAM4
Non-Sum. Mons. Reg.	0.65**	0.29*	0.66**	0.35**	0.012	0.038	0.041	0.055
Trans. Reg.	0.89**	0.49**	0.87**	0.23*	0.018	0.028	0.019	0.066
Sum. Mons. Reg.	0.92**	0.75**	0.91**	0.17*	0.026	0.034	0.027	0.050

Note. "**" and "*" represent values that passed the significance test at the 99% and 95% confidence levels, respectively.

10.1029/2024JD041899

Table 3
Same as Table 2, but for Evapotranspiration

	Temporal correlation				RMSE (mm)			
	GLDAS	ERA-interim	ERA5-land	GLEAM4	GLDAS	ERA-interim	ERA5-land	GLEAM4
Non-Sum. Mons. Reg.	0.77**	0.69**	0.64**	0.75**	19.3	18.4	20.2	19.9
Trans. Reg.	0.89**	0.83**	0.85**	0.77**	28.6	30.1	29.7	27.5
Sum. Mons. Reg.	0.84**	0.73**	0.72**	0.89**	32.9	35.3	31.8	33.2

Note. "**" and "*" represent values that passed the significance test at the 99% and 95% confidence levels, respectively.

ERA-interim data and GLEAM4 data in the SMR, SMTR, and NSMR, and slightly superior to ERA5-Land data. Therefore, the selection of GLDAS soil moisture data for this study was considered reasonably. Moreover, the significant impact of precipitation forcing data, derived from observational data, on the simulation of soil moisture is notable. In NSMR, the scarcity of observational stations compromises the precision of the precipitation. Regional variations in root zone depth may contribute to the larger errors in the GLEAM4 data.

Furthermore, both the correlation coefficient and RMSE illustrated that the evapotranspiration data from GLDAS, ERA-interim, ERA5-land, and GLEAM4 were consistent with the observed data (Table 3). Moreover, considering the overall performance in the three climate zones (SMR, SMTR, and NSMR), GLDAS was slightly superior to the other three data sets. Therefore, when the temporal resolution of observational data is insufficient for research purposes, GLDAS evapotranspiration data were a more reasonable option.

2.4. Methods

2.4.1. Determination of the Climate and Land-Surface Variables

To describe the degree of variation of the major climate and land surface variables, their relative change in amplitude each year was calculated using Equation 1:

$$\Delta X_i = X_i - X_{\min}, i = 1, 2, \ldots, n \quad (1)$$

where ΔX_i represents the change in amplitude of major climate variables, including annual mean temperature (°C) and annual precipitation (mm), as well as major land surface factors such as soil moisture (m^3 m^{-3}), land evapotranspiration (mm d^{-1}), and surface net radiation (W m^{-2}); i is the sequence number of the year in the time series of data; n is the length of the data sequence (unit: year); X_i is the annual mean (or annual accumulation) of the major climate or land surface elements in the i-th year; and $X_{\min}$ is the minimum annual mean value (or annual accumulation) of the major climate or land surface elements in the data series.

2.4.2. Definition of the Climate Space Type

To quantitatively represent the spatial discrepancy of the climate background, the climate space type can be defined by the range of the annual mean value of a given physical quantity (Zhang, Yang, et al., 2019). For example, the range of the annual mean value of a given annual precipitation or soil moisture content can be used to determine the different climate space types of precipitation or soil moisture, and then the spatial climate distribution of precipitation or soil moisture can be determined according to the climate space type. A mean precipitation of 100 mm was used to define the precipitation climate space type, and was referred to as the PXXX precipitation climate type. For example, a region with an annual mean precipitation in the range of 0–100 mm can be described as the P50 climate type and a region with an annual mean precipitation in the range of 100–200 mm can be described as the P150 climate type, with other precipitation climate types to be similarly defined. The climate space of soil moisture can also be defined in a similar way. An annual mean value of 0.01 m^3 m^{-3} was used to define the soil moisture climate spatial type, and was referred to as the SMXX soil moisture climate type. For example, the region with an annual mean soil moisture in the range of 0.095–0.105 m^3 m^{-3} can be described as the SM10 soil moisture climate type, and the region with an annual mean soil moisture in the range of 0.105–0.115 m^3 m^{-3} can be described as the SM11 soil moisture climate type. The same classification method can be used for the division of other soil moisture climate types.

2.4.3. Moisture Content Normalization Index

To facilitate a comparative analysis, it is often necessary to normalize some variables so that variables with different dimensions or orders of magnitude can be transformed into dimensionless variables or variables of the same-order magnitude. In this study, the following formula was used to normalize soil moisture data:

$$\mathrm{SM}_i = \frac{X_i\text{-}X_{\min}}{X_{\max}\text{-}X_{\min}}, i = 1, 2, \ldots, n \tag{2}$$

where SM_i is the time series value of normalized soil moisture; i is the serial number of the year of the soil moisture data in the time series; X_i is the i-th time series value of soil moisture; $X_{\min}$ is the minimum value of soil moisture in the data series; and $X_{\max}$ is the maximum value of soil moisture in the data series. The normalized soil moisture value is kept within the range of [0, 1], which more clearly reflects the variation of soil moisture and facilitates a comparison between different regions.

2.4.4. Inclination Rates of Climate and Land-Surface Elements

The climatic inclination rates of climatic and land-surface elements represent the temporal trend of specific climate factors, which are commonly used to express their responses to climate change (Zhang, Yang, et al., 2019). This kind of inclination rate is used in this study, and can be determined by a linear fitting relation as follows:

$$X = a_1 + I_c \times t \tag{3}$$

where X is the climatic and land-surface element; a_1 is the intercept of the fitting relation; I_c is the slope of the fitting relation, expressed as the climate inclination rate; and t is time (unit: yr).

The other inclination rate reflects the changing trend of climatic and land-surface elements with other climate elements, that is, the climate inclination rate varies with climatic elements, which can also be determined by the linear fitting relationship expressed in the following formula:

$$X = a_2 + I_p \times Y \tag{4}$$

where X represents climate element; a_2 is the intercept of the fitting relationship; I_p is the slope of the fitting relationship or the variation of the climate inclination rate with climate elements; and Y is the different climate element from X.

2.4.5. Sensitivity of the Inclination Rate to the Variation of Precipitation Climate Space

In regions with an obvious climate transition, the inclination rate of land-surface elements changes considerably with the precipitation climate space, and so does the degree or sensitivity of such changes. The inclination rate of land-surface elements reflects the response sensitivity of land-surface elements to climate change, while the degree of variation of the inclination rate of land-surface elements with precipitation climate space reflects the sensitivity of this inclination rate to the precipitation climate space change. The sensitivity of the inclination rate to precipitation climate space change can be determined by the linear fitting relation in Equation 5:

$$I_p = a_3 + S_I \times P \tag{5}$$

where I_p represents the variation of the inclination rate of land-surface elements with climatic elements; a_3 is the intercept of the fitting relationship; S_I stands for the slope of the fitting relationship, that is, the sensitivity of the inclination rate to the spatial variation of precipitation climate, and P is the multi-year average precipitation (unit: mm) in climate space.

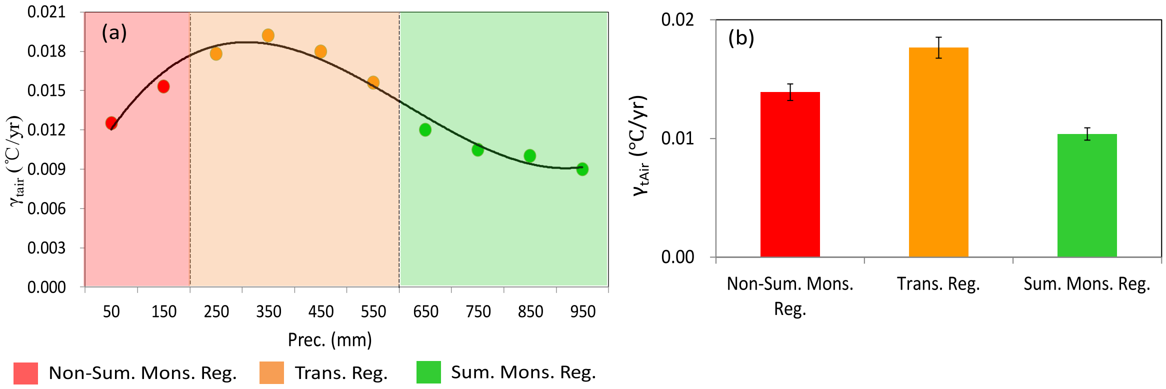

Figure 4. (a) Variation of the temperature climate inclination rate with precipitation climate space and (b) comparison of their mean values in non-summer monsoon region (NSMR), transitional region and summer monsoon region. All inclination rates passed the significance test at the 95% confidence levels.

2.4.6. Land-Atmosphere Coupling Index

The land-atmosphere coupling processes are mainly manifested as the connections between the changes in atmospheric conditions and the changes in land surface conditions, and are quantitatively represented by the land-atmosphere coupling index, which is commonly defined by a combination of evaporation and soil moisture, as shown in Equation 6 (Dirmeyer, 2011; Zeng & Xie, 2015):

$$\mathrm{CI}(s_m, e_m) = \sqrt{n}r(s_m, e_m)\sigma(e_m) \tag{6}$$

$\mathrm{CI}(s_m, e_m)$ is the land-atmosphere coupling index for the m-th month, s_m and e_m represent the soil moisture and evapotranspiration, respectively, for the m-th month. $r(s_m, e_m)$ is the correlation coefficient of a time series composed of soil moisture and evapotranspiration in the m-th month, $\sigma(e_m)$ is the standard deviation of the time series of evapotranspiration in the m-th month, n is the time length of the data (in years). It is noticeable that $CI(s_m, e_m)$ is determined jointly by $r(s_m, e_m)$ and $\sigma(e_m)$.

Furthermore, the relationship between atmospheric conditions and evapotranspiration can be represented by the correlation coefficient between evapotranspiration and the specific humidity at 2 m (Dirmeyer et al., 2013), which is represented as $r(e_m, q_m)$. Therefore, this study uses the land-atmosphere coupling index and the correlation coefficient between evapotranspiration and the air humidity to quantitatively investigate the land-atmosphere coupling characteristics in northern China, with a focus on the strong land-atmosphere coupling season (Jun–Aug).

3. Results

3.1. Climatic-Spatial Variability in the Response of Land-Atmosphere Coupling to Climate Warming

The response of land-atmosphere coupling processes to global warming tends to be significantly influenced by regional climatic conditions (Seneviratne et al., 2006). Thus, before analyzing the spatial variation characteristics of land-atmosphere coupling processes in response to global warming in northern China, it was necessary to first establish the spatial variability of climate condition changes. Figure 4 shows the variation of the temperature climate inclination rate with climate space and the mean values of the temperature climate inclination rate in the SMR, SMTR, and NSMR. The temperature climate inclination rate was distributed inconsistently across the climate space. However, the temperature climate inclination rate displayed a certain regularity with the changes in precipitation climate space, and the peak value occurred in the SMTR, which was dominated by semi-arid and semi-humid climate conditions, reaching 0.019°C yr^{-1}. The drier or wetter the region, the lower the temperature climate inclination rate, and it gradually reached a relatively stable value at 0.009°C yr^{-1} in the humid region. From a comparison of the average values of warming inclination rates in the three climate zones in northern China, it was apparent that the temperature climate inclination rates were higher in the NSMR and SMTR, with the SMTR having the highest rate of 0.018°C yr^{-1}, which was higher than the rate of 0.011°C yr^{-1} in the region affected by the summer monsoon.

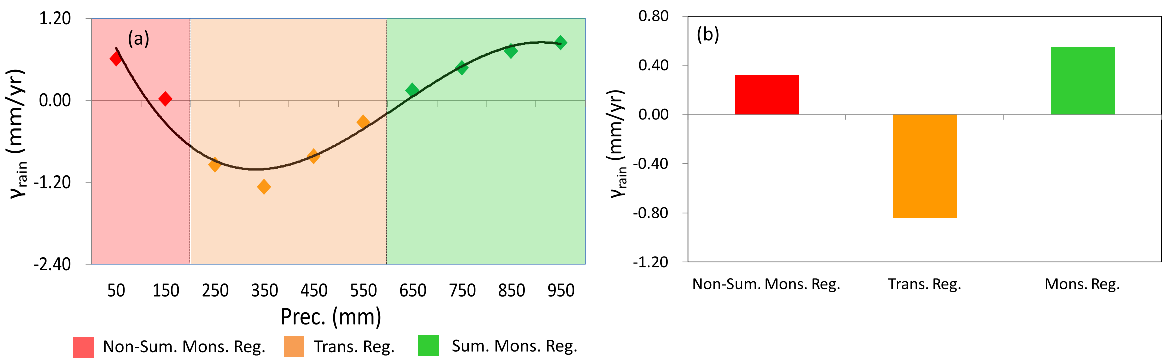

Figure 5. (a) Variation of the precipitation climate inclination rate with precipitation climate space and (b) comparison of the mean precipitation climate inclination rates in non-summer monsoon region, summer monsoon transitional region and summer monsoon region. All inclination rates passed the significance test at the 95% confidence levels.

Because the climate in arid areas is more sensitive to global warming (Koutroulis, 2018), it was expected that the warming rate would be more obvious in the NSMR and the SMTR, both of which are drier than the SMR. However, the fastest warming did not occur in the driest non-monsoon region, but in the semi-arid and semi-humid SMTR, which was an unexpected outcome. This phenomenon was considered credible because Li et al. (2015) also obtained similar results, demonstrating the special sensitivity of the response of SMTR to climate change.

In addition to temperature, precipitation is also an important spatial climate element. Its variation trend is not only closely related to land-atmosphere coupling processes, but may even affect the variation trend of temperature. For this reason, Figure 5 shows the variation of the precipitation climate inclination rate with the change of precipitation climate space and compares their average values in the NSMR, SMTR, and SMR. It can be seen from the figure that the variation of the precipitation climate inclination rate with precipitation climate space was the opposite of the regular variation of the temperature climate inclination rate with climate space shown in Figure 4. The lowest precipitation climate inclination rate (-1.27 mm yr^{-1}) was found in the SMTR, where semi-arid and sub-humid climates were dominant. In this region, the precipitation climate inclination rate gradually turned from negative to positive as the climate became drier or moister, and the inclination rate continued to increase, gradually reaching a relatively stable value of 0.85 mm yr^{-1} in humid areas. The precipitation climate inclination rates in the NSMR and SMR were both positive with values of 0.32 and 0.55 mm yr^{-1}, respectively, which indicated that the climate in the two regions was becoming wetter. In contrast, a negative precipitation climate inclination rate of -0.84 mm yr^{-1} was found in the SMTR, which indicated that the climate in this region was getting drier, with the drying trend being more noticeable than the wetting trend in the other two regions.

This unique change of the precipitation climate inclination rate with precipitation climate space was unexpected and has rarely been explicitly reported in earlier studies. However, this feature is essentially consistent with the conclusions of previous studies of the distribution pattern of precipitation change trends in China (Li et al., 2018; K. Liu et al., 2020, Y. Liu et al., 2020), which also agreed with the results of climate warming and humidification studies in arid areas of northwest China (Zhang et al., 2021). We noted that the lowest value of the precipitation climate inclination rate corresponded with the peak value of the temperature climate inclination rate (Li et al., 2015). This phenomenon suggests that in regions where the climate becomes drier, the magnitude of warming will be greater, which is theoretically reasonable. The decrease in precipitation led to a reduction in the cooling effect on the atmosphere, which can partially explain why the temperature increase in Figure 4 was more distinct in the SMTR, which was composed of semi-arid and sub-humid regions, than in the NSMR, which was dominated by an arid climate.

3.2. Climatic-Spatial Variability in the Response of Land-Atmosphere Coupling to Climate Warming

The unique features of the variation of temperature and precipitation climate inclination rates with precipitation climate space in northern China will affect the response of land-atmosphere coupling processes to global warming in this region. In land-atmosphere coupling processes, soil moisture is one of the most active land-surface physical elements. Its close mutual feedback with land-surface evapotranspiration and net radiation can in turn influence

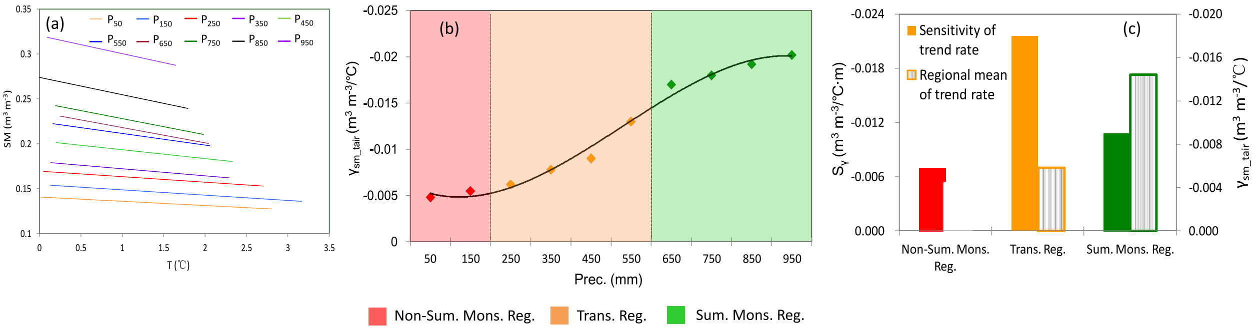

Figure 6. (a) Trends of soil moisture variation under different precipitation climate types with temperature warming, (b) changes in the inclination rate with precipitation climate space, and (c) comparison of the mean values and spatial sensitivities in panel (b) in non-summer monsoon region, summer monsoon transitional region and summer monsoon region. All inclination rates passed the significance test at the 95% confidence levels.

the changes in precipitation and temperature. Figures 6a and 6b show the variation of soil moisture with increasing temperature and the variation of the soil moisture inclination rate with precipitation climate space. Additionally, the average values and spatial sensitivity of the changing inclination rates with precipitation climate space in the NSMR, SMTR, and SMR shown in Figure 6b were compared in Figure 6c. These figures show that the warming inclination rate of soil moisture was negative, that is, the soil was drying with the increasing temperature. However, in very dry areas, the soil dried slowly and the warming inclination rate of soil moisture was maintained at about $-0.005\ m^3\ m^{-3}{}^\circ C^{-1}$. The warming inclination rate of soil moisture increased rapidly with the precipitation climate space, gradually reaching a higher stable value of about $-0.021\ m^3\ m^{-3}{}^\circ C^{-1}$ in humid regions. By comparing the mean values and sensitivities of the soil moisture warming inclination rates in the NSMR, SMTR, and SMR, we found soil drying was most noticeable in the SMR, reaching an average of $-0.017\ m^3\ m^{-3}{}^\circ C^{-1}$, followed by the SMTR with an average drying rate of $-0.007\ m^3\ m^{-3}{}^\circ C^{-1}$, and the slowest soil drying rate of only $-0.005\ m^3\ m^{-3}{}^\circ C^{-1}$ in the NSMR. The spatial sensitivity of the soil moisture warming inclination rate was most prominent in the SMTR, that is, the most substantial variation of the inclination rate with precipitation climate space occurred in this region. However, it was not very sensitive in the NSMR and SMR, indicating that the inclination rate did not vary as much with the precipitation climate space.

These analyses indicate that the soil moisture used for evaporation was more abundant under climate warming, and therefore the more humid the climate becomes, the more obvious the soil drying will be (Zaitchik et al., 2023). In arid climatic conditions, the lower soil water content limited the supply capacity for evaporation. It can be inferred from the asymptotically stable soil moisture warming inclination rate in the humid climate zone that the sensitivity of the soil moisture warming inclination rate to the variation of precipitation amount in the precipitation climate space was reduced under sufficiently humid climate conditions. The soil moisture warming inclination rate was most sensitive to the precipitation climate space in the SMTR where there was soil moisture but the soil failed to become saturated.

The changes in soil moisture content were affected by both temperature and precipitation. Figure 7 shows the variation trend of soil moisture with the increase in precipitation (Figure 7a) and its inclination rate variation with

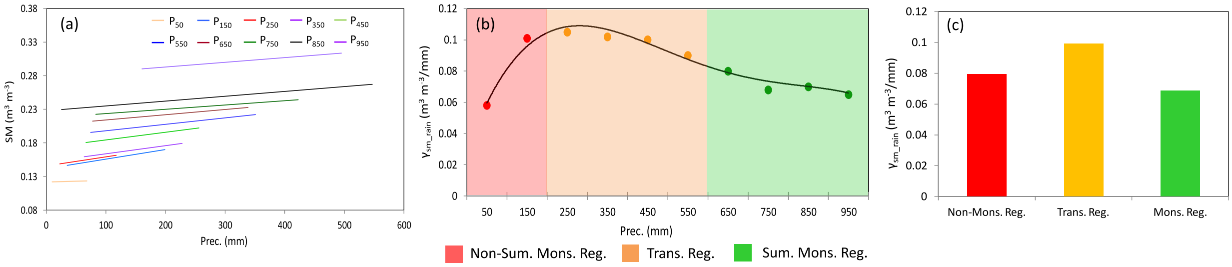

Figure 7. (a) Trends of soil moisture variation under different precipitation climate types with increasing precipitation, (b) changes in the inclination rate with precipitation climate space, and (c) comparison of the mean values in panel (b) in non-summer monsoon region, summer monsoon transitional region and summer monsoon region. All inclination rates passed the significance test at the 95% confidence levels.

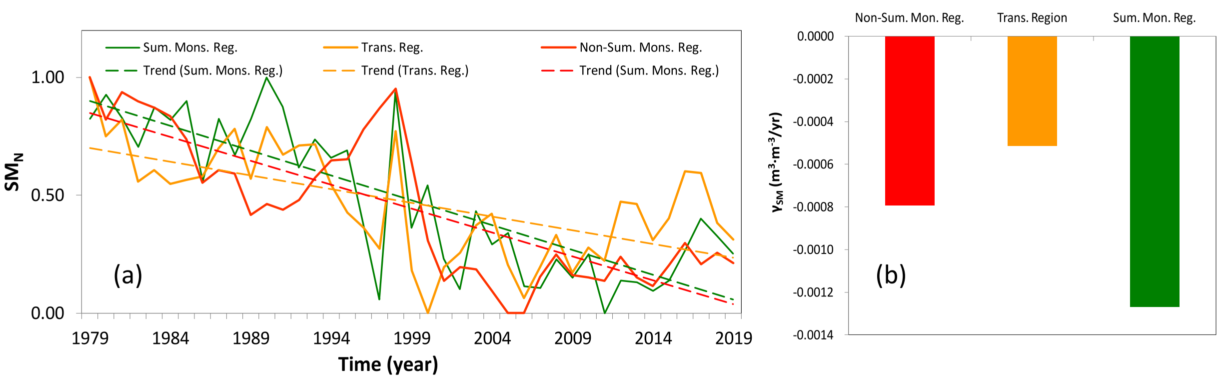

Figure 8. (a) Trends of soil moisture content variation in non-summer monsoon region, summer monsoon transitional region and summer monsoon region, and (b) a comparison of their inclination rates. All inclination rates passed the significance test at the 95% confidence levels.

precipitation climate space (Figure 7b) and Figure 7c shows a comparison of the mean values of Figure 7b in the NSMR, SMTR, and SMR. The tendency for soil moisture to increase with precipitation was prominent with the variation of precipitation climate space, but the soil moisture content increased with increasing precipitation and the soil moisture inclination rate displayed the following distribution characteristics. The peak value of the growth in the soil moisture inclination rate with precipitation was found in the SMTR, which means that the soil moisture was most sensitive to the change of precipitation amount and the most significant humidification effect occurred in this region. However, the soil moisture inclination rate tended to decrease with the increase in precipitation in drier or wetter areas, and gradually reached a relatively stable value of 0.066 $m^3\ m^{-3}\ mm^{-1}$ in humid areas. The average soil moisture inclination rates with increasing precipitation in the NSMR, SMTR, and SMR were compared and the results further confirmed that the SMTR had the highest soil moisture inclination rate of 0.099 $m^3\ m^{-3}\ mm^{-1}$, followed by the NSMR at 0.079 $m^3\ m^{-3}\ mm^{-1}$, and finally the SMR with the smallest value of only 0.068 $m^3\ m^{-3}\ mm^{-1}$. This distribution pattern is understandable because under a humid climate, soil moisture is not as sensitive to changes in precipitation as it is in a drier climate. Under a very humid climate, if the soil is saturated the soil moisture content will no longer be affected by precipitation. Overall, the influence of precipitation changes in the NSMR on soil moisture was not as obvious as those in the SMTR. This was probably because the precipitation amounts in the non-summer monsoon region were relatively low and the rain water on the ground tended to evaporate quickly. In such cases, such precipitation is unable to reach the degree of affecting soil moisture.

Changes in temperature and precipitation can simultaneously impact the climatic characteristics of soil moisture in a forceful way. As seen from Figure 8, in the NSMR, SMTR, and SMR, the normalized soil moisture content generally displayed a decreasing trend. This indicates that the changes in soil moisture were normally controlled by the changes in temperature, and the drying trend was correlated with the significant rise in temperature. However, the two periods of soil moisture change in the 1990 and 2010s were mainly controlled by changes in precipitation, corresponding to the two periods of increased precipitation (K. Liu et al., 2020, Y. Liu et al., 2020). The changing rates of soil moisture inclination in the NSMR and SMTR regions were smaller than those in the wetter SMR. This was associated with the characteristics of the regional response of soil moisture to temperature warming. Moreover, the wetter SMTR had a lower inclination rate than the drier NSMR, which was correlated with a lower rate of drying in SMR (Cheng & Huang, 2016; Deng et al., 2020).

The mutual feedback process between land evapotranspiration and soil moisture is the core linkage in land-atmosphere coupling. Figure 9 shows the variation of land evapotranspiration with an increase in soil moisture (Figure 9a) and the variation of the soil moisture inclination rate with precipitation climate space (Figure 9b). Figure 9c shows a comparison of the mean values of the changes in inclination rate with precipitation climate space shown in Figure 9b between the NSMR, SMTR, and SMR. It is apparent that the inclination rate of land evapotranspiration with an increase in soil moisture not only varied significantly with the precipitation climate space, but also converted from a positive to a negative value. The conversion interval occurred just within the SMTR. Specifically, the inclination rate was positive in the drier NSMR or land evapotranspiration increased with the increase in soil moisture content, and the drier the climate became the more obvious the increase was.

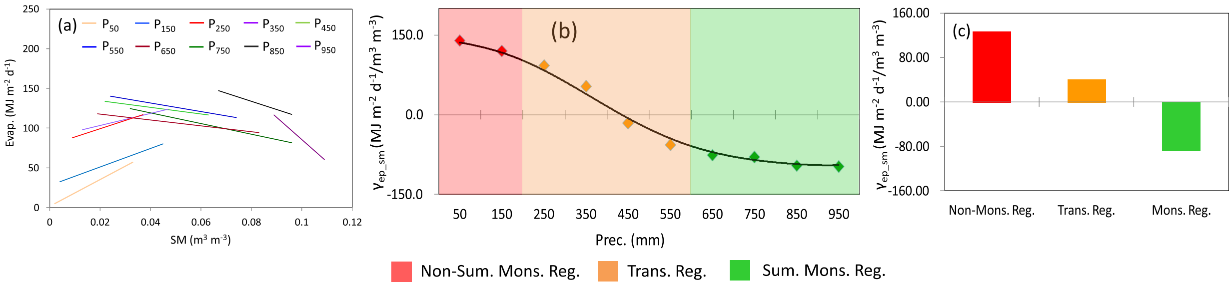

Figure 9. (a) Variation of land evapotranspiration under different precipitation climate types with increasing soil moisture, (b) changes in the inclination rate with precipitation climate space, and (c) a comparison of the mean values in panel (b) in non-summer monsoon region, summer monsoon transitional region and summer monsoon region. All inclination rates passed the significance test at the 95% confidence levels.

Conversely, the inclination rate gradually became negative in the wetter SMR, indicating that land evapotranspiration weakened with increasing soil moisture content. The wetter the climate the more obvious the weakening was, until a relatively stable value was reached.

These conversion characteristics are related to the response of land evapotranspiration to energy and moisture. Under conditions with insufficient soil moisture, the increase in land evapotranspiration often depends on the increase in soil moisture (Rihani et al., 2015), but when the soil moisture content is sufficient, the increase in land evapotranspiration is often determined by temperature and surface radiation conditions (Polson & Hegerl, 2017). Therefore, in arid areas free from the influence of the summer monsoon, land-surface evapotranspiration is mainly dominated by moisture constraints. With an increase in soil moisture, land evapotranspiration could increase naturally, and the inclination rate of land evapotranspiration would therefore be positive. In contrast, in the humid SMR, land-surface evapotranspiration was mainly under the control of energy factors. However, in the context of climate warming, a decrease in soil moisture content occurred alongside the warming temperature in the humid areas of the SMR (Figure 6). In this region, the characteristics of decreasing land evapotranspiration reflected the effects of the temperature rise on soil moisture reduction. Both constraint mechanisms could coexist in the SMTR, and the moisture and energy constraints were competitive to a certain extent. The inclination rate of land evapotranspiration therefore also underwent a positive to negative conversion.

Surface net radiation provides the energy for land-surface heat and evaporation, and it is also the main constraint for land evapotranspiration. The response of surface net radiation to soil moisture is also one of the important linkages in land-atmosphere coupling. The variation of surface net radiation with the increase in soil moisture content and the change in the soil moisture inclination rate with the precipitation climate space are given in Figures 10a and 10b, respectively, while the average values of the inclination rates given in Figure 10b are compared between the NSMR, SMTR, and SMR in Figure 10c. It can be seen that, as with land evapotranspiration, the surface net radiation inclination rate with increasing soil moisture also converted from positive to negative values in the SMTR. This inclination rate gradually became a positive value in drier NSMR where the surface net radiation strengthened as soil moisture was added, while in the more humid SMR the inclination rate

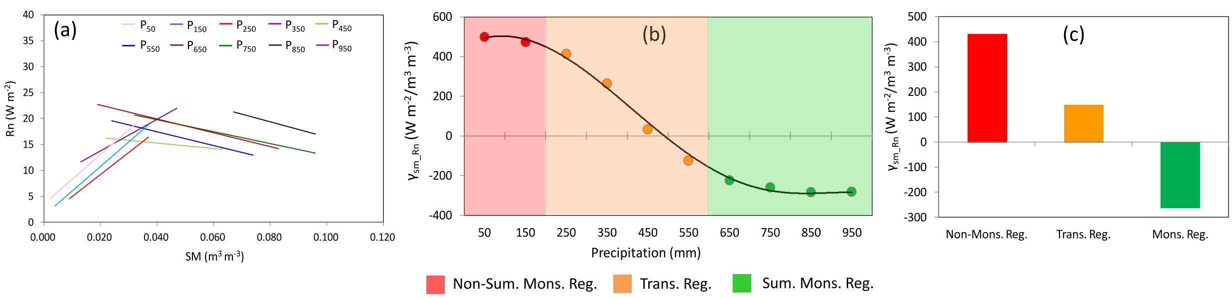

Figure 10. (a) Trends of surface net radiation variation under different precipitation climate types with increasing soil moisture, (b) changes in the inclination rate with precipitation climate space, and (c) comparison of the mean values of the inclination rates in panel (b) in non-summer monsoon region, summer monsoon transitional region and summer monsoon region. All inclination rates passed the significance test at the 95% confidence levels.

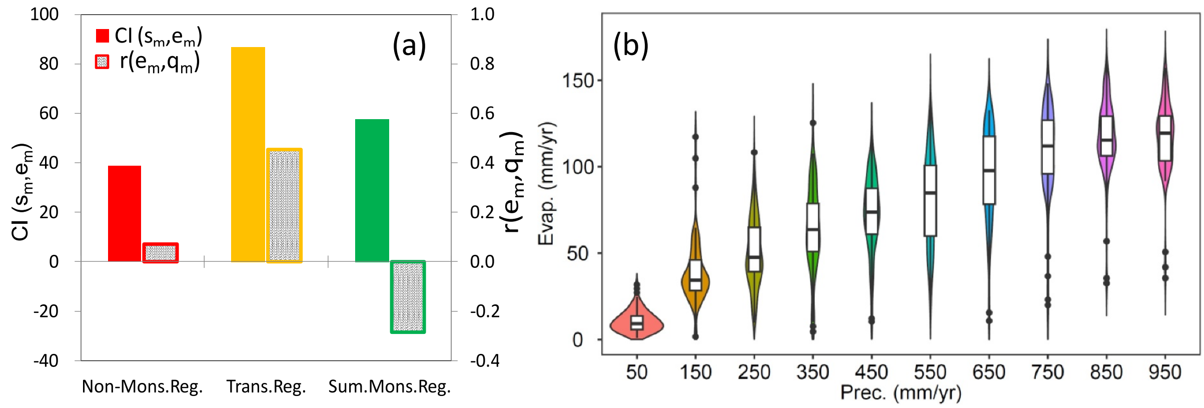

Figure 11. (a) Comparison of the coupling index (CI) and the correlation coefficients ($r(e_m, q_m)$) between evapotranspiration and specific humidity in non-summer monsoon region, summer monsoon transitional region and summer monsoon region, (b) boxplot of summer evapotranspiration in different precipitation climate types.

gradually became negative. This indicated that the surface net radiation weakened with the increasing soil moisture content and a relatively stable value was gradually reached.

The distribution of the surface net radiation inclination rate with soil moisture was linked to the mechanisms by which soil moisture influences surface net radiation through the surface albedo and the transfer of solar radiation to the Earth's surface. In the drier NSMR, the influence of soil moisture on the surface net radiation could be adjusted by the surface short-wave albedo. The greater the soil moisture, the smaller the surface albedo; the smaller the albedo, the stronger the surface net radiation. However, in the humid SMR, the albedo was not sensitive to the change of soil moisture, and the influence of soil moisture on the surface net radiation was dominated by solar radiation. The greater the soil moisture, the more clouds and water vapor there are; the more clouds and water vapor, the less solar radiation reaches the surface; and the lower the incoming solar radiation, the weaker the surface net radiation (Deng et al., 2020).

The CI(s_m, e_m) derived from soil moisture and evapotranspiration reveals varying degrees of land-atmosphere coupling across precipitation climate types (Figure 11a). It shows the most pronounced coupling intensity in the SMTR, followed by SMTR, with NSMR displaying the least significant coupling. The SMTR primarily governed by semi-arid climatic conditions, experiences sufficient summer precipitation and relatively high soil moisture content (0.15–0.3 $m^3\ m^{-3}$) (Zhang et al., 2023), facilitating stronger land-atmosphere coupling with a coupling index of 87.0. The SMR, despite having sufficient soil moisture, exhibits weaker land-atmosphere coupling due to insufficient energy to evaporate all the soil moisture into the atmosphere. Moreover, the NSMR, characterized by arid climatic conditions and scarce precipitation, experiences a deficit in soil moisture, resulting in weak land-atmosphere coupling.

Furthermore, the $r(e_m, q_m)$ shows the influence of soil moisture on specific humidity is minimal in the NSMR, with a correlation coefficient of 0.07 that does not pass the significance test at the 95% confidence level (Figure 11b). However, specific humidity exhibits high sensitivity to soil moisture responses in the SMTR, with a correlation coefficient of 0.45, passing the significance test at the 99% confidence level. It is worth noting that high values of specific humidity in the SMR are often influenced by anomalies in summer monsoon water vapor transport (Huang et al., 2011). Evapotranspiration, primarily regulated by energy, shows a negative correlation with water vapor transport, $r(e_m, q_m)$, as high values of water vapor transport correspond to low values of evapotranspiration (Zeng & Xie, 2015). As shown in Figure 11b, in the SMR, the median and upper and lower quartiles of evapotranspiration change little with the variation of precipitation climate types, indicating a small land-atmosphere water vapor pressure difference and weak land-atmosphere coupling strength. In contrast, in the SMTR, evapotranspiration changes significantly with the variation of precipitation climate types, indicating a large land-atmosphere water vapor pressure difference and strong land-atmosphere coupling strength. In the NSMR, the land-atmosphere coupling strength remains relatively weak due to the small evapotranspiration.

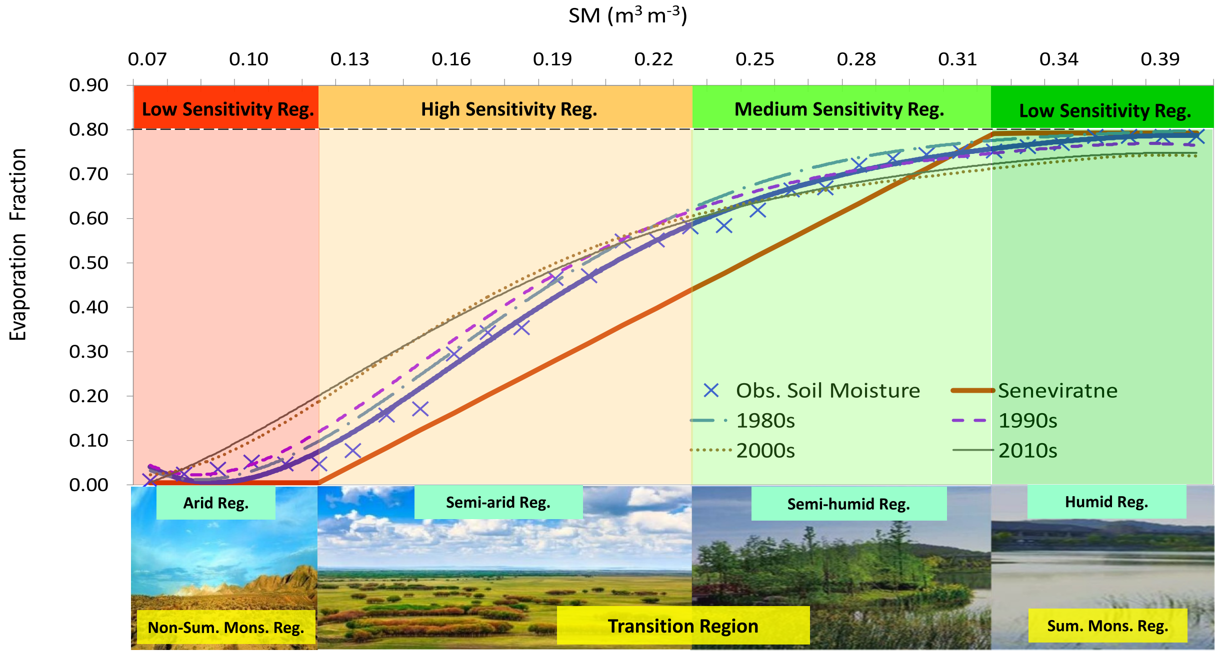

Figure 12. Distribution curve of the land evaporative fraction with soil moisture climate space in northern China versus the Seneviratne ideal curve (The blue solid line is based on observed data, and the results for the 4 decades are based on GLDAS).

4. Discussion

The results of this study indicated that the spatial variations of land-atmosphere coupling processes in response to climate warming in northern China are associated with the degree of influence of energy and moisture on land-atmosphere coupling processes. The spatial differences in the response of land-atmosphere coupling processes to climate warming could therefore be distinguished by the parameters that can characterize energy and moisture. The evapotranspiration ratio $EF = LE/(LE + SH)$, where LE is the latent heat flux and SH is the sensible heat flux, is not only an important parameter for surface energy balance and ecological processes, but a critical index to comprehensively measure the relationships between land surface energy and water content distribution (Crago, 1996). It can be used to determine the different spatial distributions of land surface energy and water content.

Figure 12 compares the observed distribution curve of the land evaporative fraction with soil moisture climate space in northern China and the ideal distribution curve of Seneviratne et al. (2010). The two curves approach each other and eventually converge, showing that the land evaporative fraction to the spatial changes of soil moisture in arid and humid areas are very low: approximately 0 and 0.8, respectively. Only in the semi-arid and semi-humid climate transitional zone, where the soil moisture is in its climate space range of 0.120–0.315 $m^3\ m^{-3}$, does the land evaporative fraction have a more prominent sensitivity to the spatial variation of soil moisture. This reflects the significant constraint of the energy and hydrological cycles in the climate transitional region. The difference between the two curves is that the Seneviratne ideal curve is a simple linear variation, while the actual curve is a more complex quintic fitting function, which can be expressed by the following fitting relation formula:

$$\Psi = -2e^{-7}\theta^5 + 2e^{-5}\theta^4 - 9e^{-4}\theta^3 + 0.016\theta^2 - 0.07\theta + 0.096 \tag{7}$$

where θ is soil moisture ($m^3\ m^{-3}$) and Ψ is the land evaporative fraction, which is dimensionless with values of 0–1. The larger the ratio, the more abundant the water content, and the more obvious the energy constraints.

The shape of the variation curve and the quintic fitting function of Equation 7 show apparently that in the climate transitional zone, the curve of the variation of land surface evaporative fraction with soil moisture climate space had an inflection point, which was approximately the dividing line between semi-arid and semi-humid areas.

10.1029/2024JD041899

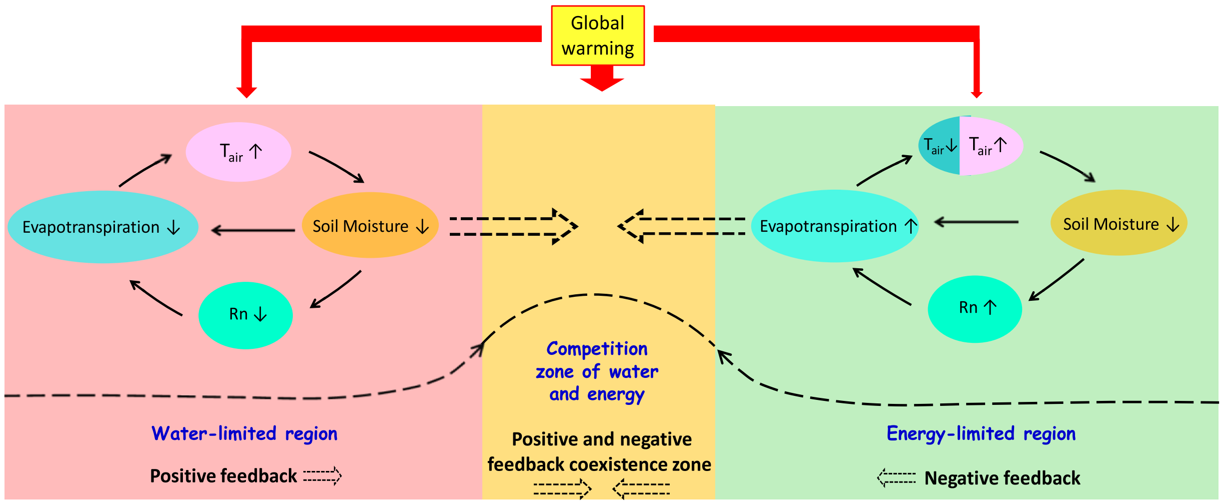

Figure 13. Schematic diagram of the response mechanisms of land-atmosphere coupling processes to climate warming as a function of climate space conversion and transition over northern China.

Before the inflection, the land evaporative fraction changed more rapidly with the climate space of soil moisture; after the inflection, the land evaporative fraction varied more slowly with the climate space of soil moisture. Therefore, the sensitive region of the land evaporative fraction could be subdivided into high and medium sensitivity portions.

Furthermore, from the evaporative fraction variation curves of the four decades, it is evident that the evaporative fraction's response to increasing soil moisture shows similar patterns between the 1980 and 1990s, and between the 2000 and 2010s. Notably, the evaporative fraction in the first 20 years is significantly lower than in the latter 20 years in arid and semi-arid regions. As soil moisture levels approach those of semi-humid regions, the evaporative fraction in the first 20 years gradually exceeds that of the latter 20 years.

This shift is mainly due to changes in precipitation trends. L. Zhang et al. (2022), Q. Zhang et al. (2022) found that around the year 2000, the arid and semi-arid regions in this study experienced a significant eastward moistening trend, while the semi-humid and humid regions saw a decrease in precipitation. This precipitation shift resulted in increased latent heat and evaporative fraction in the arid and semi-arid regions during the latter 20 years, and a decrease in the evaporative fraction in the semi-humid and humid regions. This underscores the intricate relationship between soil moisture, precipitation trends, and evaporative fraction across different climate zones.

The different feedback mechanisms between climate and land-surface physical quantities in northern China could be summarized and classified on the basis of the different sensitivity types of climate space divided by land evapotranspiration. As shown in Figure 13, the response mechanism of the land-atmosphere coupling processes to climate warming differed NSMR, SMTR and SMR, and it changed with the variation of climate space. In the NSMR, the response mechanism was moisture-constrained: the increasing temperature led to a decrease in soil moisture, which in turn caused a decline in land-surface evapotranspiration and net radiation. This would increase temperatures and aggravate climate warming. A relatively complete positive feedback process therefore occurred (Eltahir, 1998; Eltahir & Bras, 1996). In contrast, in the SMR, the response mechanism took the form of an energy-constrained mechanism: the rise in temperature reduced soil moisture, accelerated vegetation growth, and decreased surface albedo; further leading to an increase in net surface radiation and an increase in land-surface evapotranspiration and net radiation, followed by a decrease in temperature, which would inhibit climate warming, thus forming a relatively complete negative feedback process (Diffenbaugh et al., 2007). It may be because of these opposite feedback mechanisms in arid and humid areas that arid areas are more sensitive to global warming than humid areas, which leads to a larger magnitude of warming in arid areas.

Whether the land-atmosphere coupling processes had a positive or negative feedback on climate warming was mainly determined by the response relationship of land-surface evapotranspiration and net radiation to soil moisture. If they were positively correlated, it was a positive feedback mechanism, otherwise it was a negative feedback mechanism. In the SMTR, due to the influence of seasonal changes and interannual fluctuations of

10.1029/2024JD041899

climate the moisture and energy constraint mechanisms were intermittent. The two constraint mechanisms were competitive, and therefore this region was defined as the "moisture and energy competition constraint zone" or "coexistence of positive and negative feedback mechanisms zone."

In summary, based on the above analyses, the response of land-atmosphere coupling processes to climate warming was determined by the features of the climate space type, and a transformation was also possible with the changes of climate space. This finding was not only consistent with the mutual feedback relationship between climate and land-surface physical quantities in northern China, which was revealed in the previous section, but also in line with the prevailing theories and logical speculations.

Moreover, this study compared the ensemble mean of soil moisture and evapotranspiration simulated by the four GLDAS models with observational data. The results showed that their comprehensive performance in terms of correlation and root mean square error in northern China was superior to that of three reanalysis data sets (ERA-Interim, ERA5-Land, and GLEAM4). This indicates that, compared to single-model results in reanalysis data sets, the multi-model ensemble mean of GLDAS can reduce errors caused by differences in model structures and minimize errors arising from different model parameters. This demonstrates that the ensemble mean of multi-model results remains an important alternative for reducing simulation errors. On the other hand, over the past few years, with the application of higher-density station data and data assimilation systems (Albergel et al., 2018; Probst & Mauser, 2022), along with the use of more advanced land surface models, model parameter optimization, and bias correction methods (Cucchi et al., 2020; Decker et al., 2012; K. Liu et al., 2020, Y. Liu et al., 2020; Weedon et al., 2014), the performance of reanalysis data derived from single models has significantly improved. Results driven by mainstream forcing data using single models can reflect land-atmosphere coupling relationships in northern China (e.g., the strong coupling between precipitation and soil moisture) (Yang et al., 2017; Zeng et al., 2021; Zhang, Yang, et al., 2019), providing data support for large-scale regional land-atmosphere coupling process studies (Rivera, 2014). However, it is important to emphasize that for research on hydrological processes in smaller-scale mountainous areas and river basins, the demand for higher-quality forcing data remains urgent (Albergel et al., 2018; Yang et al., 2017).

5. Conclusions

Northern China is a region with intense land-atmosphere coupling. This article has utilized various observational and internationally recognized reanalysis data sets, along with methods such as climate inclination rates and land-atmosphere coupling indices, to investigate the response variability of land-atmosphere coupling processes to climate warming and the response mechanisms of the coupling processes between land evapotranspiration and soil moisture, and between surface net radiation and soil moisture to the spatial change of precipitation climate space (Figure 14). The research conclusions drawn are as follows:

The peak value of the temperature climate inclination rate occurred in the SMTR, and then decreased toward drier or wetter regions. In contrast, the precipitation climate inclination rate was lowest in the SMTR, but was higher in drier or wetter regions. After a certain moisture content was reached in climate space, both the temperature and precipitation inclination rates were maintained at stable levels.

The soil moisture inclination rate linked to warming in northern China was generally negative. In the NSMR, the soil dried out more slowly due to the limited soil moisture available for evaporation. In the SMTR, the rate of soil moisture loss was faster than in NSMR. In the humid SMR, the soil dried out the fastest but at a relatively steady rate, which was the result of there being sufficient soil moisture for evaporation. However, the soil moisture inclination rate with increasing precipitation was positive, with its peak value found in the SMTR. This phenomenon indicated that the soil moisture was most sensitive to the change of precipitation in the SMTR. Therefore, the actual variation of soil moisture was generally controlled by changes in temperature, although there was also a notable influence from the varying precipitation.

The increasing inclination rates of the land-surface evapotranspiration and net radiation along with soil moisture had a unique variation in climate space. In the drier NSMR, the inclination rates became positive gradually, while in the wetter SMR the rates were negative. This was related to the responses of the land-surface evapotranspiration and net radiation to the energy and hydrological cycles. In NSMR, land evapotranspiration was mainly confined by soil moisture while the surface net radiation was controlled by surface albedo; in SMR, land evapotranspiration was mainly limited by energy but the surface net radiation was determined by the solar

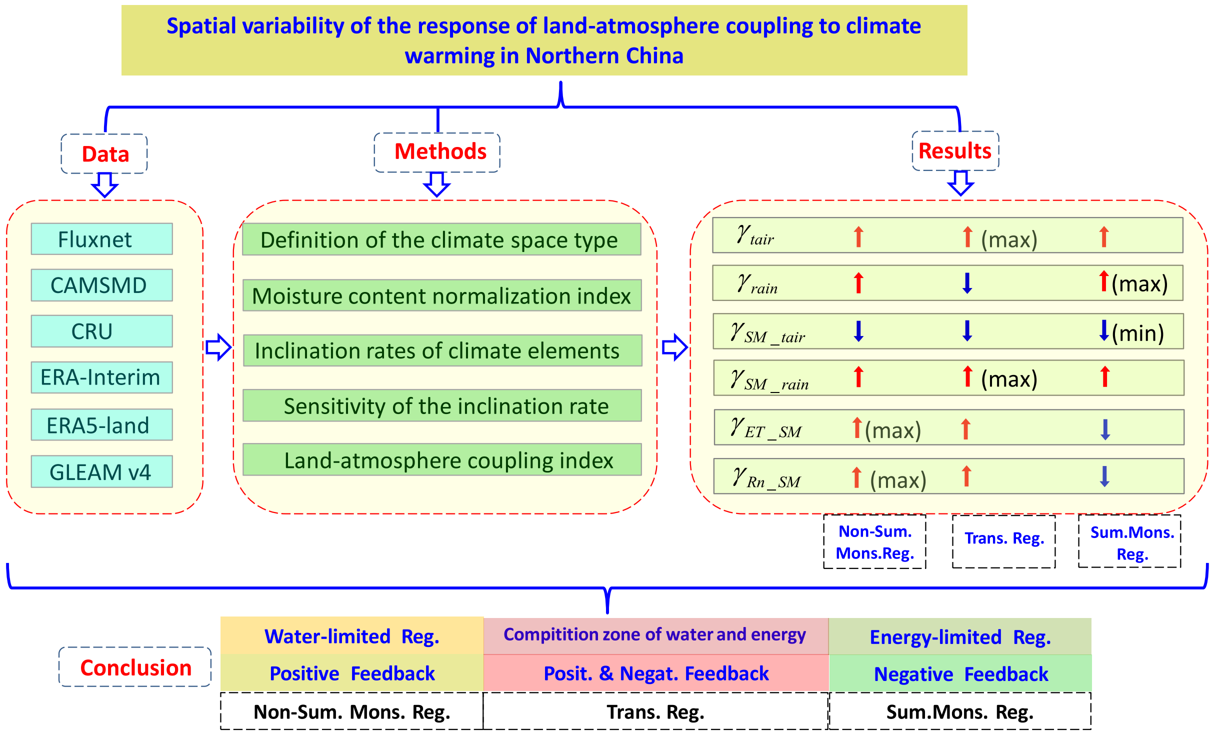

Figure 14. A sketch of the data, methods, results and conclusions in the study. (Note: "↑" and "↓" represent increasing inclination rates and decreasing inclination rates, respetively).

radiation to the surface. However, in the SMTR the two constraint mechanisms competed against each other, resulting in positive and negative variations in the inclination rates of the land-surface evapotranspiration and net radiation.

The distribution curve of the land evaporative fraction with soil moisture climate space in northern China was close to the Seneviratne ideal change curve (Seneviratne et al., 2010). Both curves were not sensitive to changes in soil moisture in arid and humid regions, but they had a very strong sensitivity to soil moisture changes in the transitional zones of semi-arid and semi-humid climates. The difference existing between the two curves was that the Seneviratne ideal curve was a simple linear relationship, while the actual curve was a quintic fitting curve and its sensitivity could be subdivided into two sub-regions of high and medium sensitivity by the inflection point of the curve. This study investigated the relationship between some key elements of land-atmosphere coupling, without involving other elements, and therefore the understanding of land-atmosphere coupling processes was not very comprehensive. Because the precipitation formation mechanism is very complex, we did not directly consider the land water cycle process and the mutual feedback relationship between precipitation and land physical quantities in the spatial distribution diagram. Additionally, there was a need to ensure sufficient climate and land surface data, but the data sources used for this study were not uniform, which might have affected the accuracy of the conclusions. These issues need to be overcome in future studies.

Data Availability Statement

The ECMWF Re-Analysis project data-Interim (ERA-Interim) data and ERA5-land data can be downloaded from ECMWF website (Berrisford et al., 2011; Hersbach et al., 2020). The GLEAM4 data can be obtained from the Global Land Evaporation Amsterdam Model (GLEAM) website (Martens et al., 2017). The temperature and precipitation data can be obtained from the Climatic Research Unit (CRU) website (Harris et al., 2020). The Global Land Data Assimilation (GLDAS) data can be obtained from the NASA Goddard Earth Sciences Data and Information Services Center (GES DISC) (Rodell et al., 2004). The FLUXNET data can be downloaded from the Lawrence Berkeley National Laboratory (USA, Pastorello et al., 2021).

Acknowledgments

This study was supported by the National Natural Science Foundation of China (Grant 42230611, 41630426, 41875020) and Natural Science Foundation of Gansu Province (Grant 24JRRA724). We sincerely thank all three anonymous reviewers for their very thoughtful and constructive comments and suggestions.

References

Albergel, C., Dutra, E., Munier, S., Calvet, J., Munoz-Sabater, J., de Rosnay, P., & Balsamo, G. (2018). ERA-5 and ERA-interim driven ISBA land surface model simulations: Which one performs better? *Hydrology and Earth System Sciences*, *22*(6), 3515–3532. https://doi.org/10.5194/hess-22-3515-2018

Berrisford, P., Kallberg, P., Kobayashi, S., Dee, D., Uppala, S., Simmons, A., et al. (2011). Atmospheric conservation properties in ERA-Interim [Dataset]. *ECMWF-interim land dataset*, *137*(659), 1381–1399. https://doi.org/10.1002/qj.864

Blay-Carreras, E., Gonzalez, P., Arellano, D., Coster, J., Darbieu, O., Darbieu, C., et al. (2014). Role of the residual layer and large-scale subsidence on the development and evolution of the convective boundary layer. *Atmospheric Chemistry and Physics*, *14*(9), 4515–4530. https://doi.org/10.5194/acp-14-4515-2014

Cheng, S., & Huang, J. (2016). Enhanced soil moisture drying in transitional regions under a warming climate. *Journal of Geophysical Research: Atmospheres*, *121*(6), 2542–2555. https://doi.org/10.1002/2015JD024559

Crago, R. D. (1996). Conservation and variability of the evaporative fraction during the daytime. *Journal of Hydrology*, *180*(1–4), 173–194. https://doi.org/10.1016/0022-1694(95)02903-6

Cucchi, M., Weedon, G. P., Amici, A., Bellouin, N., Lange, S., Müller Schmied, H., et al. (2020). WFDE5: Bias-adjusted ERA5 reanalysis data for impact studies. *Earth System Science Data*, *12*(3), 2097–2120. https://doi.org/10.5194/essd-12-2097-2020

Decker, M., Brunke, M. A., Wang, Z., Sakaguchi, K., Zeng, X., & Bosilovich, M. G. (2012). Evaluation of the reanalysis products from GSFC, NCEP, and ECMWF using flux tower observations. *Journal of Climate*, *25*(6), 1916–1944. https://doi.org/10.1175/JCLI-D-11-00004.1

Deng, Y., Wang, S., Bai, X., Luo, G., Wu, L., Cao, Y., et al. (2020). Variation trend of global soil moisture and its cause analysis. *Ecological Indicators*, *110*, 105939. https://doi.org/10.1016/j.ecolind.2019.105939

Diffenbaugh, N., Pal, J., Giorgi, F., & Gao, X. (2007). Heat stress intensification in the Mediterranean climate change hotspot. *Geophysical Research Letters*, *34*(11), L11706. https://doi.org/10.1029/2007GL030000

Dirmeyer, P. A. (2011). The terrestrial segment of soil moisture–climate coupling. *Geophysical Research Letters*, *38*(16), 1–5. https://doi.org/10.1029/2011GL048268

Dirmeyer, P. A., Jin, Y., Singh, B., & Yan, X. (2013). Trends in land–atmosphere interaction from CMIP5 Simulations. *Journal of Hydrometeorology*, *14*(3), 829–849. https://doi.org/10.1175/JHM-D-12-0107.1

Eltahir, E. (1998). A soil moisture–rainfall feedback mechanism: 1. Theory and observations. *Water Resources Research*, *34*(4), 765–776. https://doi.org/10.1029/97WR03499

Eltahir, E., & Bras, R. (1996). Precipitation recycling. *Reviews of Geophysics*, *34*(3), 367–378. https://doi.org/10.1029/96RG01927

Emori, S. (1998). The interaction of cumulus convection with soil moisture distribution: An idealized simulation. *Journal of Geophysical Research*, *103*(D8), 8873–8884. https://doi.org/10.1029/98JD00426

Evans, J., Pitman, A., & Cruz, F. (2011). Coupled atmospheric and land surface dynamics over Southeast Australia: A review, analysis and identification of future research priorities. *International Journal of Climatology*, *31*(12), 1758–1772. https://doi.org/10.1002/joc.2206

Feng, S., & Fu, Q. (2013). Expansion of global drylands under a warming climate. *Atmospheric Chemistry and Physics*, *13*(19), 10081–10094. https://doi.org/10.5194/acp-13-10081-2013

Findell, K., & Eltahir, E. (2003a). Atmospheric controls on soil moisture–boundary layer interactions. Part I: Framework development. *Journal of Hydrometeorology*, *4*(3), 552–569. https://doi.org/10.1175/1525-7541(2003)004<0552:ACOSML>2.0.CO;2

Findell, K., & Eltahir, E. (2003b). Atmospheric controls on soil moisture–boundary layer interactions. Part II: Feedbacks within the continental United States. *Journal of Hydrometeorology*, *4*(3), 570–583. https://doi.org/10.1175/1525-7541(2003)004<0570:ACOSML>2.0.CO;2

Freire, L., & Dias, N. (2013). Residual layer effects on the modeling of convective boundary layer growth rates with a slab model using FIFE data. *Journal of Geophysical Research: Atmospheres*, *118*(23), 12869–12878. https://doi.org/10.1002/jgrd.50796

Guo, Z., & Dirmeyer, P. (2013). Interannual variability of land–atmosphere coupling strength. *Journal of Hydrometeorology*, *14*(5), 1636–1646. https://doi.org/10.1175/JHM-D-12-0171.1

Han, L., Zhang, Q., Zhang, Z., Jia, J., Wang, Y., Huang, T., & Cheng, Y. (2021). Drought area, intensity and frequency changes in China under climate warming, 1961–2014. *Journal of Arid Environments*, *193*, 104596. https://doi.org/10.1016/j.jaridenv.2021.104596

Harris, I., Jones, P. D., Osborn, T. J., & Lister, D. H. (2014). Updated high-resolution grids of monthly climatic observations – The CRU TS3.10 dataset. *International Journal of Climatology*, *34*(3), 623–642. https://doi.org/10.1002/joc.3711

Harris, I., Osborn, T. J., Jones, P., & Lister, D. (2020). Version 4 of the CRU TS monthly high-resolution gridded multivariate climate dataset [Dataset]. *Climate Research Unit Data Sets*, *7*(1), 109. https://doi.org/10.1038/s41597-020-0453-3

Hersbach, H., Bell, B., Berrisford, P., Hirahara, S., Horányi, A., Muñoz-Sabater, J., et al. (2020). The ERA5 global reanalysis [Dataset]. *Climate Data Store*, *146*(730), 1999–2049. https://doi.org/10.1002/qj.3803

Huang, J., Guan, X., & Ji, F. (2012). Enhanced cold-season warming in semi-arid regions. *Atmospheric Chemistry and Physics*, *12*, 4627–4653. Discussions. https://doi.org/10.5194/acp-12-5391-2012

Huang, R., Chen, J., & Liu, Y. (2011). Interdecadal variation of the leading modes of summertime precipitation anomalies over Eastern China and its association with water vapor transport over East Asia. *Chinese Journal of Atmospheric Sciences*, *35*(4), 589–606. https://doi.org/10.3878/j.issn.1006-9895.2011.04.01

Jung, M., Reichstein, M., & Bondeau, A. (2009). Towards global empirical upscaling of FLUXNET eddy covariance observations: Validation of a model tree ensemble approach using a biosphere model. *Biogeosciences*, *6*(10), 2001–2013. https://doi.org/10.5194/bg-6-2001-2009

Koster, R., Dirmeyer, P., Guo, Z., Gordon, B., Ed, C., Peter, M., et al. (2004). Regions of strong coupling between soil moisture and precipitation. *Science*, *305*(5687), 1138–1140. https://doi.org/10.1126/science.1100217

Koutroulis, A. (2018). Dryland changes under different levels of global warming. *Science of the Total Environment*, *655*, 482–511. https://doi.org/10.1016/j.scitotenv.2018.11.215

Li, H., Zhang, Q., Yue, P., Zhang, L., Niu, X., Zhang, H., et al. (2021). Temporal duration of the East Asian summer monsoon substantially affects surface energy exchange over the summer monsoon transition zone of China. *Journal of Climate*, *34*, 4643–4660. https://doi.org/10.1175/JCLI-D-20-0102.1

Li, W., Jiang, Z., Zhang, X., & Li, L. (2018). On the emergence of anthropogenic signal in extreme precipitation change over China. *Geophysical Research Letters*, *45*(17), 9179–9185. https://doi.org/10.1029/2018GL079133

Li, Y., Huang, J., Ji, M., & Ran, J. (2015). Dryland expansion in Northern China from 1948 to 2008. *Advances in Atmospheric Sciences*, *32*(6), 870–876. https://doi.org/10.1007/s00376-014-4106-3

Liu, K., Nie, G., & Zhang, S. (2020a). Study on the spatiotemporal evolution of temperature and precipitation in China from 1951 to 2018. *Advances in Earth Science*, *35*, 1113–1126. https://doi.org/10.11867/j.issn.1001-8166.2020.102

Liu, L., Zhang, R., & Zuo, Z. (2014). Intercomparision of spring soil moisture among multiple reanalysis datasets over Eastern China. *Journal of Geophysical Research: Atmospheres*, *119*, 1–11. https://doi.org/10.1002/2013JD020940
Liu, Y., Huang, J., Shi, G., Takamura, T., Khatri, P., Bi, J., et al. (2011). Aerosol optical properties and radiative effect determined from sky-radiometer over Loess Plateau of Northwest China. *Atmospheric Chemistry and Physics*, *11*(22), 11455–11463. https://doi.org/10.5194/acp-11-11455-2011
Liu, Y., Yang, Z., Lin, P., Zheng, Z., & Xie, S. (2020b). Comparison and evaluation of multiple land surface products for the water budget in the Yellow River Basin. *Journal of Hydrology*, *584*, 124534. https://doi.org/10.1016/j.jhydrol.2019.124534
Martens, B., Miralles, D. G., Lievens, H., van der Schalie, R., de Jeu, R. A. M., Fernández-Prieto, D., et al. (2017). GLEAM v3: Satellite-based land evaporation and root-zone soil moisture [Dataset]. *GLEAM*, *10*(5), 1903–1925. https://doi.org/10.5194/gmd-10-1903-2017
Min, L., Min, Q., & Du, Y. (2022). Evaluation of model summertime boundary layer cloud development over complex terrain in New York State. *Weather and Forecasting*, *37*(12), 2195–2207. https://doi.org/10.1175/WAF-D-21-0172.1
Miralles, D., Holmes, T., de Jeu, R., Gash, J., Meesters, A., & Dolman, A. (2011). Global land-surface evaporation estimated from satellite-based observations. *Hydrology and Earth System Sciences*, *15*(2), 453–469. https://doi.org/10.5194/hess-15-453-2011
Ni, Y., Qiu, B., Guo, W., Li, L., Chen, J., Tian, X., et al. (2024). Shift of soil moisture-temperature coupling exacerbated 2022 compound hot-dry event in Eastern China. *Environmental Research Letters*, *19*(1), 014059. https://doi.org/10.1088/1748-9326/ad178c
Pastorello, G., Pastorello, G., Trotta, C., Canfora, E., Chu, H., Christianson, D., et al. (2021). The FLUXNET2015 dataset and the ONEFlux processing pipeline for eddy covariance data [Dataset]. *The Data Portal serving the FLUXNET community*. https://fluxnet.org/data/fluxnet2015-dataset/
Polson, D., & Hegerl, G. C. (2017). Strengthening contrast between precipitation in tropical wet and dry regions. *Geophysical Research Letters*, *44*(1), 365–373. https://doi.org/10.1002/2016GL071194
Probst, E., & Mauser, W. (2022). Evaluation of ERA5 and WFDE5 forcing data for hydrological modelling and the impact of bias correction with regional climatologies: A case study in the Danube River Basin. *Journal of Hydrology: Regional Studies*, *40*(12), 101023. https://doi.org/10.1016/j.ejrh.2022.101023
Rihani, J., Chow, F., & Maxwell, R. (2015). Isolating effects of terrain and soil moisture heterogeneity on the atmospheric boundary layer: Idealized simulations to diagnose land-atmosphere feedbacks. *Journal of Advances in Modeling Earth Systems*, *7*(2), 915–937. https://doi.org/10.1002/2014MS000371
Rivera, J. (2014). A comparison of GLDAS soil moisture anomalies against standardized precipitation index and multi-satellite estimations over South America. *Journal of Hydrometeorology*, *16*(1), 158–171. https://doi.org/10.1175/JHM-D-13-0190.1
Rodell, M., Houser, P., Jambor, U., Gottschalck, J., Mitchell, K., Meng, C. J., et al. (2004). The global land data assimilation system [Dataset]. *GES DISC*, *85*(3), 381–394. https://doi.org/10.1175/bams-85-3-381
Schumacher, D., Keune, J., van Heerwaarden, C., Arellano, J., Teuling, A., & Miralles, D. (2019). Amplification of mega-heatwaves through heat torrents fuelled by upwind drought. *Nature Geoscience*, *12*(9), 712–717. https://doi.org/10.1038/s41561-019-0431-6
Seneviratne, S., Corti, T., Davin, E., Hirschi, M., Jaeger, E., Lehner, I., et al. (2010). Investigating soil moisture–climate interactions in a changing climate: A review. *Earth-Science Reviews*, *99*(3–4), 125–161. https://doi.org/10.1016/j.earscirev.2010.02.004
Seneviratne, S., Donat, M., Pitman, A., Knutti, R., & Wilby, R. (2016). Allowable CO_2 emissions based on regional and impact-related climate targets. *Nature*, *529*(7587), 477–483. https://doi.org/10.1038/nature16542
Seneviratne, S., Lüthi, D., Litschi, M., & Schär, C. (2006). Land-atmosphere coupling and climate change in Europe. *Nature*, *443*(7108), 205–209. https://doi.org/10.1038/nature05095
Sheffield, J., Goteti, G., & Wood, E. (2006). Development of a 50-year high-resolution global dataset of meteorological forcings for land surface modeling. *Journal of Climate*, *19*(13), 3088–3111. https://doi.org/10.1175/JCLI3790.1
Taylor, C., Gounou, A., Guichard, F., Harris, P., Ellis, R., Couvreux, F., & De Kauwe, M. (2011). Frequency of Sahelian storm initiation enhanced over mesoscale soil-moisture patterns. *Nature Geoscience*, *4*(7), 430–433. https://doi.org/10.1038/ngeo1173
Wang, A., & Zeng, X. (2015). Global hourly land surface air temperature datasets: Inter-comparison and climate change. *International Journal of Climatology*, *35*(13), 3959–3968. https://doi.org/10.1002/joc.4257
Wang, Y., Yuan, X., Liu, Y., & Wang, W. (2024). Skillful seasonal prediction of the 2022–23 mega soil drought over the Yangtze River basin by combining dynamical climate prediction and copula analysis. *Environmental Research Letters*, *6*, 064019. https://doi.org/10.1088/1748-9326/ad4978
Weedon, G., Balsamo, G., Bellouin, N., Gomes, S., Best, M., & Viterbo, P. (2014). The WFDEI meteorological forcing data set: WATCH forcing data methodology applied to ERA-interim reanalysis data. *Water Resources Research*, *50*(9), 7505–7514. https://doi.org/10.1002/2014WR015638
Wei, Q., Zhang, C., Fu, G., & Zhou, H. (2015). Global Land Data Assimilation System data assessment using a distributed biosphere hydrological model. *Journal of Hydrology*, *528*(11), 652–667. https://doi.org/10.1016/j.jhydrol.2015.07.011
Wetzel, P., Argentini, S., & Boone, A. (1996). Role of land surface in controlling daytime cloud amount: Two case studies in the GCIP-SW area. *Journal of Geophysical Research*, *101*(D3), 7359–7370. https://doi.org/10.1029/95JD02134
Yang, F., Lu, H., Yang, K., Wang, W., Li, C., Han, M., et al. (2017). Evaluation of multiple forcing data sets for precipitation and shortwave radiation over mainland China. *Hydrology and Earth System Sciences*, *21*(11), 5805–5821. https://doi.org/10.5194/hess-21-5805-2017
Zaitchik, B., Rodell, M., Biasutti, M., & Seneviratne, S. (2023). Wetting and drying trends under climate change. *Nature Water*, *1*(6), 502–513. https://doi.org/10.1038/s44221-023-00073-w
Zeng, J., Yuan, X., Ji, P., & Shi, C. (2021). Effects of meteorological forcings and land surface model on soil moisture simulation over China. *Journal of Hydrometeorology*, *603*, 126978. https://doi.org/10.1016/j.jhydrol.2021.126978
Zeng, J., & Zhang, Q. (2012). A comparative study of the characteristics of the clear sky land surface processes over the different underlying surfaces in the northern part of China during July–September 2008. *Acta Oceanologica Sinica*, *70*, 821–836. https://doi.org/10.11676/qxxb2012.068
Zeng, Y., & Xie, Z. (2015). Projection and evaluation of the land–atmosphere coupling strength over China by CMIP5 models. *Climatic and Environmental Research (in Chinese)*, *20*(3), 337–346. https://doi.org/10.3878/j.issn.1006-9585.2015.14242
Zhang, H., Zhang, L., & Pak, B. (2011). Comparing surface energy, water and carbon cycle in dry and wet regions simulated by a land-surface model. *Theoretical and Applied Climatology*, *104*(3–4), 511–527. https://doi.org/10.1007/s00704-010-0364-x
Zhang, H., Zhang, Q., Yue, P., Zhang, L., Liu, Q., Qiao, S., & Yan, P. (2016). Aridity over a semi-arid zone in northern China and responses to the East Asian summer monsoon: Aridity response to EASM Margin. *Journal of Geophysical Research: Atmospheres*, *121*(23), 13901–13918. https://doi.org/10.1002/2016jd025261
Zhang, L., Sha, S., Zhang, Q., Zhao, F., Zhao, J., Li, H., et al. (2023). Investigating the coupling relationship between soil moisture and evaporative fraction over China's transitional climate zone. *Hydrology*, *10*(12), 221. https://doi.org/10.3390/hydrology10120221

10.1029/2024JD041899

Zhang, L., Zhang, H., Zhang, Q., Li, Y., & Zhao, J. (2017). On the potential application of land surface models for drought monitoring in China. *Theoretical and Applied Climatology*, *128*(3–4), 649–665. https://doi.org/10.1007/s00704-016-1730-0

Zhang, L., Zhang, Q., Zhang, H., Yue, P., Li, H., Wang, J., et al. (2022a). Environmental factors driving evapotranspiration over a grassland in a transitional climate zone in China. *Meteorological Applications*, *29*(3), e2066. https://doi.org/10.1002/met.2066

Zhang, Q., Qiao, L., Yue, P., & Li, Y. (2019). The energy mechanism controlling the continuous development of a super-thick atmospheric convective boundary layer during continuous summer sunny periods in an arid area. *Chinese Science Bulletin*, *64*(15), 1637–1650. https://doi.org/10.1360/N972018-01014

Zhang, Q., Yang, J., Duan, X., Ma, P., Lu, G., Zhu, B., et al. (2022b). The eastward expansion of the climate humidification trend in northwest China and the synergistic influences on the circulation mechanism. *Climate Dynamics*, *59*(7–8), 2481–2497. https://doi.org/10.1007/s00382-022-06221-4

Zhang, Q., Yang, J., Wang, W., Ma, P., Lu, G., Liu, X., et al. (2021). Climatic warming and humidification in the arid region of northwest China: Multi-scale characteristics and impacts on ecological vegetation. *Journal of Meteorological Research*, *35*(1), 113–127. https://doi.org/10.1007/s13351-021-0105-3

Zhang, Q., Yang, Z., Hao, X., & Yue, P. (2019). Conversion features of evapotranspiration responding to climate warming in transitional climate regions in Northern China. *Journal of Meteorological Research*, *52*(7–8), 3891–3903. https://doi.org/10.1007/s00382-018-4364-3

Zhang, Q., Zeng, J., Yue, P., Zhang, L., Wang, W., & Wang, R. (2020). On the land-atmosphere interaction in the summer monsoon transition zone in East Asia. *Theoretical and Applied Climatology*, *141*(3–4), 1165–1180. https://doi.org/10.1007/s00704-020-03239-8

Zhang, Q., Zhang, L., Huang, J., Zhang, L., Wang, L., & Sha, S. (2014). Spatial distribution of surface energy fluxes over the Loess Plateau in China and its relationship with climate and the environment. *Science China Earth Sciences*, *57*(9), 2135–2147. https://doi.org/10.1007/s11430-014-4881-9

Zheng, Y., Kumar, A., & Niyogi, D. (2015). Impacts of land–atmosphere coupling on regional rainfall and convection. *Climate Dynamics*, *44*(9–10), 2383–2409. https://doi.org/10.1007/s00382-014-2442-8

Zhou, S., Williams, A., Berg, A., Cook, B., Zhang, Y., Hagemann, S., et al. (2019). Land–atmosphere feedbacks exacerbate concurrent soil drought and atmospheric aridity. *Proceedings of the National Academy of Sciences of the United States of America*, *116*(38), 18848–18853. https://doi.org/10.1073/pnas.1904955116

Zuo, Z., & Zhang, R. (2016). Influence of soil moisture in eastern China on East Asian summer monsoon. *Advances in Atmospheric Sciences*, *33*(2), 151–163. https://doi.org/10.1007/s00376-015-5024-8